# Integration of Three-Phase LLC Resonant Converter and Full Bridge Converter for Hybrid Modulated Multi-Outputs Topology

Guangdi Li, *Member, IEEE*, Dongsheng Yang, *Senior Member, IEEE*, Bowen Zhou, *Member, IEEE*, Yan-Fei Liu, *Fellow, IEEE*, Huaguang Zhang, *Fellow, IEEE*

***Abstract*—A multi-outputs DC-DC topology based on hybrid modulation of pulse frequency modulation and phase shift is proposed in this paper. The proposed hybrid modulated multi-outputs converter is derived from the integration of a three-phase LLC resonant converter and the full bridge converter. With the hybrid modulation, the multi outputs are controlled independently free from cross regulation, and isolated from each other. With the three-phase interleaving operation, the resonant currents can be reduced and thus the efficiency will be improved. Furthermore, the output current ripple of the main output voltage is reduced, as a consequence, the lifetime of the output filter capacitor is extended and the reliability is reinforced. What's more, the number of the power switches are reduced and zero-voltage-switching of the power switches can be achieved within the entire load range by the proposed integrated topology. All of the above-mentioned features of the proposed converter will lead to a compact, efficient and cost-effective design. Finally, a 1.4kW triple-outputs laboratory prototype is built and tested to validate the feasibility and effectiveness of the proposed converter.**

***Index Terms*—Three-phase LLC resonant converter, full bridge converter, multi-outputs DC-DC converter, hybrid modulation.**

## I. INTRODUCTION

Multi-outputs DC-DC converters are found widely used in various applications, such as telecommunication power supplies, consumer electronics, renewable energy systems, battery chargers, and EVs, etc [1-5]. The multi-outputs converters are a kind of converters whose output voltages are derived from single-input converter, which show higher power density, lower system cost with reduced power switches compared to the several single-output DC-DC converters solutions. The commonly multi-outputs DC-DC converters are derived from the classical DC-DC converters, such as Buck, Boost, Cuk, etc.

[6-8] introduce some commonly used high frequency isolated DC-DC converters, among the various DC-DC converters with high frequency isolation, full bridge converter and LLC resonant converter are two types of converters that attract great interests of research for their soft-switching performance, high efficiency and high-power density. The full bridge converter [9, 10], whose output voltage is controlled by the phase angle between the bridge branches, can achieve zero-voltage switching (ZVS) without additional auxiliary circuit, as a result, the main features of the full bridge converter include high efficiency and high-power density. However, the full bridge converter has several drawbacks including: the ZVS operation will lose under light load conditions, which leads to decreased efficiency and high electro-magnetic interference (EMI) [11]; the diodes of the secondary side operate in hard-switching and the parasitic oscillation across the rectifier increases the voltage stress of devices and causes output noise [9]; a large series inductance will be needed to achieve the ZVS operation, which will cause duty cycle loss and high voltage spikes on the secondary side rectifiers [12]. Some counter measures have been proposed to mitigate the aforementioned constraints [13, 14]. However, these counter measures need extra clamp circuits which will decrease the power density.

The resonant converters [15, 16], whose output voltage is regulated by the switching frequency. Compared to the full bridge converters, the resonant converters can achieve soft-switching operation within the entire load range by the resonance of the resonant capacitor and the resonant inductor. The LLC resonant converters are widely used as the DC-DC stage due to the superior performance [17-19]. Nevertheless, the resonant converters have also some drawbacks including: the resonant current is usually large which will increase the conduction loss and decrease the efficiency [20]; the large output current ripple is also large which will shorten the lifetime of the output capacitor and degrade the reliability of the power converters [21]. In order to decrease the resonant current, the multi-phase resonant converters have been presented [22-25]. Thanks to the multi-phase architecture, the converters have advantages of lower resonant current and reduced output current ripple allowing small-size filter requirement. Among the various multi-phase DC-DC converters, the three-phase architecture is one of the most

*Manuscript received January 02, 2021; revised August 03, 2021 and October 20, 2021; accepted December 22, 2021. This work was supported in part by the State Key Laboratory of Alternate Electrical Power System with Renewable Energy Sources under Grant LAPS21007, in part by Guangdong Basic and Applied Basic Research Foundation, in part by the Fundamental Research Funds for the Central Universities under Grant N2104014 and N180415004, in part by the National Key R&D Program of China under Grant 2018YFB1700500, in part by National Natural Science Foundation of China under Grant U1908217, in part by the Liaoning Revitalization Talents Program under Grant XLYC1902055. (*Corresponding author: Dongsheng Yang*.)

Guangdi Li, Dongsheng Yang, Bowen Zhou, Huaguang Zhang are with College of Information Science and Engineering, Northeastern University, Shenyang, P.R. CHINA. (e-mail: liguangdi@mail.neu.edu.cn, yangdongsheng@mail.neu.edu.cn, zhoubowen@mail.neu.edu.cn, hgzhang@ieee.org)

Yan-Fei Liu is with with the Department of Electrical and Computer Engineering, Queen's University, Kingston, ON K7L 3N6, Canada. (e-mail: yanfei.liu@queesu.ca)

This article has been accepted for publication in a future issue of this journal, but has not been fully edited. Content may change prior to final publication. Citation information: DOI 10.1109/JESTPE.2021.3139905, IEEE Journal of Emerging and Selected Topics in Power Electronics



popular multi-phase architectures which have been studied in [26-28]. It has been proved in [29] that the three-phase interleaved LLC resonant converter can achieve automatic current sharing by interconnecting the primary sides into a common Y node [30] and the secondary sides into a common Y-node [24]. Furthermore, the three inductors and transformers can be integrated into one magnetic component [29], which can increase the power density.

A variety of multi-outputs converters have been reported in recent literatures. [31] presents a multi-outputs topology derived methodology for single-input-multi-output applications based on single-switched non-isolated DC-DC converters. With the presented topological construction method, one can obtain a variety of multi-outputs converters based on buck, boost, Cuk, SEPIC, etc. However, the derived multi-outputs converters suffer from the hard-switching operation and non-isolation. [32] presents a secondary-side modulated DC-DC topology with high frequency isolation which can achieve ZVS over a wide load range. The secondary-side modulated structure can be extended to provide multi-outputs and the multi-outputs are controlled independently and isolated from each other. However, the presented converter can't achieve ZVS over the full load range, and moreover, the secondary-side is changed into an active rectifier which will increase the control complexity and system cost.

In order to alleviate the aforementioned constraints and limitations, this paper proposes a hybrid modulated multi-outputs DC-DC topology. The proposed converter is derived from integrating the three-phase LLC resonant converter and full bridge converter. Hybrid modulation of pulse frequency modulation (PFM) and phase shift control is used in the proposed converter. One of the contributions is that the output voltages of the proposed topology are controlled by the pulse frequency and the phase shift angles. Furthermore, the other contribution is that the three-phase LLC resonant converter has smaller resonant current and output current ripples, which will increase the system efficiency. Moreover, the multi-output voltages are isolated from each other by the high frequency transformer and soft-switching operation is achieved without requiring additional auxiliary circuit within the entire load range. Therefore, the proposed converter has a compact, efficient and cost-effective topology with reduced numbers of power switches.

This paper is organized as follows. The proposed topology, circuit configuration description and operational principles analysis are exhibited in Section II. The characteristics and design considerations of the proposed multi-outputs converter are analyzed in Section III, which demonstrates that the multi outputs are controlled independently without cross regulation. Section VI exhibits the experimental results, which validate the feasibility and effectiveness of the proposed topology. Finally, the conclusions are made from the investigation in section V.

## II. PROPOSED HYBRID MULTI-OUTPUTS CONVERTER AND OPERATION PRINCIPLES

### *A.Derivation of Proposed Hybrid Modulated Multi-Outputs Converter*

The resonant converter and the full bridge converter are two different kinds of commonly used high frequency isolated DC-DC converters. The output voltage of the resonant converter is modulated by the switching frequency, while the output voltage of the full bridge converter is modulated by the phase shift between the bridge branches irrelevant to the switching frequency. The three-phase LLC resonant DC-DC converter which is commonly used in high power level is shown in Fig. 1, the three-phase LLC resonant DC-DC converter can achieve automatic current sharing by interconnecting the primary sides into a common Y-node and the secondary sides into a common Y-node, which has been proved in [29, 30]. Fig. 1 (b) shows the voltages between the midpoints of the bridge branches which are symmetric square waves, and can be used as the input voltage in the full bridge converter.

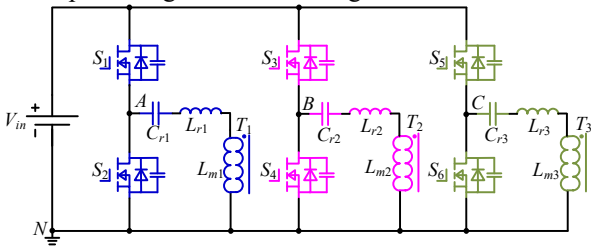


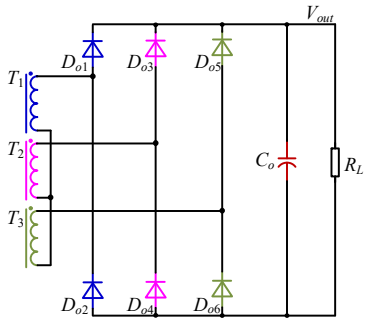


(a)

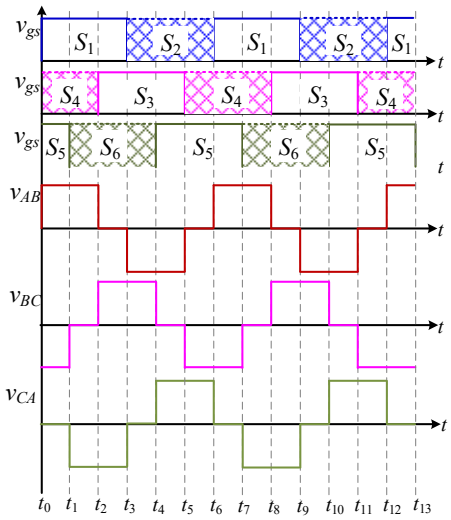


(b)

This article has been accepted for publication in a future issue of this journal, but has not been fully edited. Content may change prior to final publication. Citation information: DOI 10.1109/JESTPE.2021.3139905, IEEE Journal of Emerging and Selected Topics in Power Electronics



Fig. 1 Circuit diagram of three-phase LLC resonant DC-DC converter. (a) Three-phase LLC resonant DC-DC converter, (b) Voltages between the midpoints of bridge branches.

The multi-outputs converter is derived from the integration of the three-phase LLC resonant DC-DC converter and the full bridge DC-DC converter, which is shown in Fig. 2. Fig. 2 (a) presents a dual outputs circuit topology that the main output voltage $V_{out}$ is derived from the three-phase LLC resonant DC-DC converter, bridge $A$ and $B$ form a full bridge DC-DC converter and the additional auxiliary output voltage $V_{aux}$ is the output voltage of the full bridge DC-DC converter. Fig. 2 (b) presents a triple outputs circuit topology that the main output $V_{out}$ is derived from the three-phase LLC resonant DC-DC converter, bridge $A$, $B$ and $C$ form two full bridge DC-DC converters and two additional auxiliary output voltages $V_{aux1}$ and $V_{aux2}$ are the output voltages the two full bridge DC-DC converters. Fig. 2 (c) presents a quadruple outputs circuit topology which has a main output voltage $V_{out}$ and three additional auxiliary output voltages $V_{aux1}$, $V_{aux2}$ and $V_{aux3}$. The proposed multi-outputs converter features attributes of lower cost and higher power density without cross regulation by the combination of the three-phase LLC resonant DC-DC converter and the full bridge DC-DC converter.

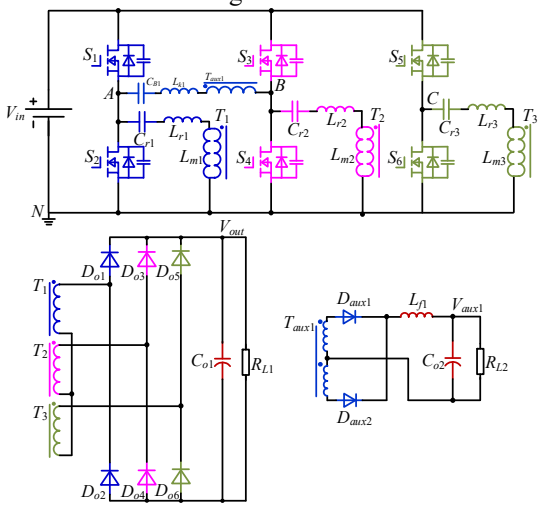


(a)

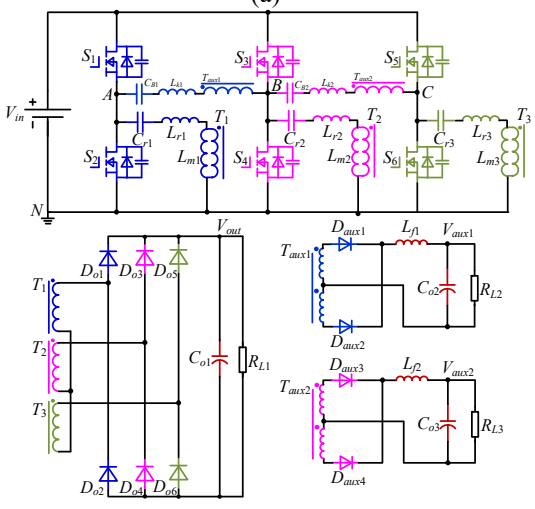


(b)

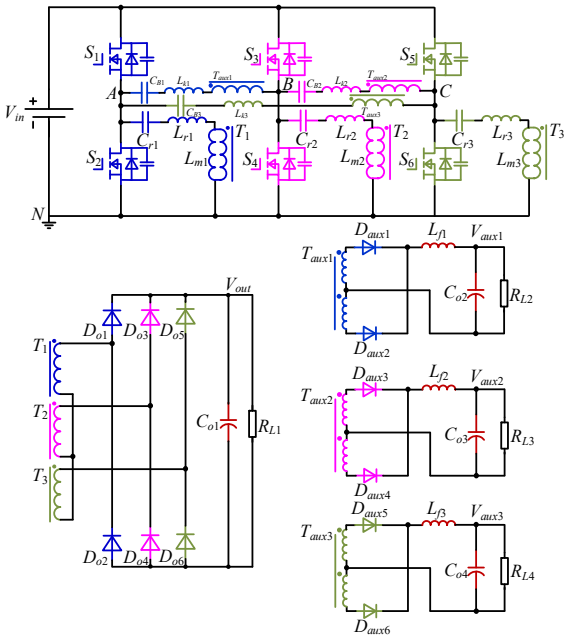


(c)

Fig. 2 Topology derivation based on modulated three-phase LLC resonant DC-DC converter and full bridge converter. (a) Topology of dual outputs, (b) topology of triple outputs, (c) topology of quadruple outputs.

This paper takes the topology of triple outputs as shown in Fig. 2 (b) as example to analyze the proposed multi-outputs converter, the output voltage $V_{out}$ is regulated by the switching frequency and the two additional auxiliary output voltage $V_{aux1}$ and $V_{aux2}$ will be left unregulated as the phase shift angles between two bridge branches are 120°. As shown in Fig. 2 (b), MOSFETs $S_1$, $S_2$, $S_3$, $S_4$, $S_5$ and $S_6$ are used to form a two-level three-phase structure. Three resonant capacitors $C_{r1}$, $C_{r2}$ and $C_{r3}$, three resonant inductors $L_{r1}$, $L_{r2}$ and $L_{r3}$, and three magnetizing inductance $L_{m1}$, $L_{m2}$ and $L_{m3}$ form a three-phase LLC resonant tank. Two dc blocking capacitor $C_{B1}$ and $C_{B2}$ and transformers $T_{axu1}$ and $T_{aux2}$ with leakage inductance $L_{k1}$ and $L_{k2}$ consist of two full bridge converters.

### *B. The Operational Principles of the Proposed Hybrid Modulated Multi-Outputs Converter*

The proposed hybrid multi-outputs converter is derived from integrating the three-phase LLC resonant converter and the full bridge converter, and the operational principles is the similar to the resonant converter and the full bridge converter. The proposed converter is modulated by the pulse frequency with pulse width 0.5. Fig. 3 and Fig. 4, respectively, shows the operational modes and the principal waveforms of the proposed converter. In Fig. 4, $v_{gs1}$, $v_{gs2}$, $v_{gs3}$, $v_{gs4}$, $v_{gs5}$, and $v_{gs6}$ are the gate-driving signals for the power switches $S_1$, $S_2$, $S_3$, $S_4$, $S_5$, and $S_6$, respectively. $i_{Lr1}$, $i_{Lr2}$, $i_{Lr3}$ are the resonant currents, and $i_{Lk1}$, $i_{Lk2}$ are the currents of the full bridge converters. $i_D$ is the output current ripple of the three-phase resonant converter. The output voltage $V_{out}$ is regulated by the switching frequency, while in order to get better current sharing performance of the three-phase LLC resonant converter, the phase shift angles between the two bridge branches $\varphi_1$ and $\varphi_2$ are designed to be 120°.

This article has been accepted for publication in a future issue of this journal, but has not been fully edited. Content may change prior to final publication. Citation information: DOI 10.1109/JESTPE.2021.3139905, IEEE Journal of Emerging and Selected Topics in Power Electronics



For sake of simplicity, some assumptions are made, listed as follows:

1) the deadband intervals of MOSFETs are ignored;

2) the two full bridge converters are designed to be operated at continuous conduction mode;

4) the values of the three-phase resonant tank are assumed to be equal: the resonant capacitors $C_{r1}$, $C_{r2}$ and $C_{r3}$ are assumed to be the same, $C_{r1}=C_{r2}=C_{r3}=C_r$; the resonant inductors $L_{r1}$, $L_{r2}$ and $L_{r3}$ are assumed to be the same, $L_{r1}=L_{r2}=L_{r3}=L_r$; the magnetizing inductance $L_{m1}$, $L_{m2}$ and $L_{m3}$ are assumed to be the same, $L_{m1}=L_{m2}=L_{m3}=L_m$;

5) the transformer $T_1$, $T_2$ and $T_3$ have a turn ratio of $n=n_1=n_2=n_3=N_{p1}/N_{s1}$, the transformer $T_{\text{aux1}}$ have a turn ratio of $n_{\text{aux1}}=N_{p\_aux1}/N_{s\_\text{aux1}}$, the transformer $T_{\text{aux2}}$ have a turn ratio of $n_{\text{aux2}}=N_{p\_\text{aux2}}/N_{s\_\text{aux2}}$;

6) the conducting voltage drop and equivalent resistance of output-rectified diodes are ignored.

7) the phase shift $\varphi_1$ and $\varphi_2$ between the bridge branches are designed to be 120°.

*Interval 1 [$t_0 \le t < t_1$; see Fig. 3 (a)]:* This interval starts when switch $S_1$ turns on and switch $S_2$ turns off at $t_0$. Before $t_0$, switch $S_4$ and $S_5$ has already conducted. The resonant inductors resonate with the resonant capacitors, therefore the resonant currents $i_{Lr1}$, $i_{Lr2}$ and $i_{Lr3}$ vary in the sinusoidal waveform by resonance. The input voltages of the resonant tanks $A$ phase and $C$ phase are $+V_{in}$, while the input voltage of the resonant tank $B$ phase is 0. And the rectifier diodes $D_{o1}$, $D_{o4}$ and $D_{o5}$ conduct during this mode. The magnetizing current $i_{Lm1}$ and $i_{Lm3}$ increase linearly by the clamped voltage, while $i_{Lm2}$ decreases linearly. In the full bridge converters, the voltage $v_{AB}$ between point $A$ and $B$ is $+V_{in}$, and the current $i_{Lk1}$ increases linearly. The voltage $v_{BC}$ between point $B$ and $C$ $v_{BC}$ is $-V_{in}$, and the current $i_{Lk2}$ decreases linearly. The currents of the full bridge converter are expressed as follows.

$$\begin{cases} i_{Lk1}(t) = i_{Lk1}(t_0) + \dfrac{V_{in} - n_{aux1}V_{aux1}}{L_{k1} + n_{aux1}^2 L_{f1}}(t - t_0) \\ i_{Lk2}(t) = i_{Lk2}(t_0) + \dfrac{V_{in} - n_{aux2}V_{aux2}}{L_{k2} + n_{aux2}^2 L_{f2}}(t - t_0) \end{cases} \tag{1}$$

*Interval 2 [$t_1 \le t < t_2$; see Fig. 3 (b)]:* This interval starts when switch $S_5$ turns off and switch $S_6$ turns on at $t_1$. Switch $S_1$ and $S_4$ has already conducted before $t_1$. The resonant inductors go on resonating with the resonant capacitors, and the resonant currents $i_{Lr1}$, $i_{Lr2}$, and $i_{Lr3}$ vary in the sinusoidal waveform. The input voltage of resonant tank $A$ is $+V_{in}$, and the input voltages of resonant tank $B$ and $C$ is $+V_{in}$. The rectifier diodes $D_{o1}$, $D_{o4}$ and $D_{o5}$ conduct during this mode. And the magnetizing current $i_{Lm1}$ and $i_{Lm3}$ increase linearly by the clamped voltage, and the magnetizing current $i_{Lm2}$ decreases linearly. In the full bridge converters, the voltage $v_{AB}$ between point $A$ and $B$ $v_{AB}$ is $+V_{in}$, and the current $i_{Lk1}$ goes on increasing; while the voltage $v_{BC}$ between point $B$ and $C$ $v_{BC}$ is 0, and the rectifier diodes $D_{aux3}$ and $D_{aux4}$ are conducting simultaneously. The capacitor $C_{B2}$ and the inductor $L_{k2}$ begin to resonate. The currents are expressed as follows.

$$\begin{cases} i_{Lk1}(t) = i_{Lk1}(t_1) + \dfrac{V_{in} - n_{aux1}V_{aux1}}{L_{k1} + n_{aux1}^2 L_{f1}}(t - t_1) \\ i_{Lk2}(t) = \dfrac{-V_{in} - v_{CB2}(t_1)}{Z_{B2}}\sin\left(\omega_{B2}(t - t_1)\right) + i_{Lk2}(t_1)\cos\left(\omega_{B2}(t - t_1)\right) \end{cases} \tag{2}$$

*Interval 3 [$t_2 \le t < t_3$; see Fig. 3 (c)]:* This interval starts when switch $S_4$ turns off and switch $S_3$ turns on at $t_2$. The switch $S_1$ and $S_6$ has already conducted before $t_2$. The resonant currents $i_{Lr1}$, $i_{Lr2}$ and $i_{Lr3}$ vary in the sinusoidal waveform by resonance. The input voltages of the resonant tank phase $A$ is $+V_{in}$, while the input voltages of the resonant tank phase $B$ and phase $C$ is 0. The rectifier diode $D_{o2}$, $D_{o3}$ and $D_{o6}$ conduct during this mode. And the magnetizing current $i_{Lm1}$ and $i_{Lm2}$ increase linearly by the clamped voltage, while the magnetizing current $i_{Lm3}$ decreases linearly. In the full bridge converters, the voltage $v_{AB}$ between point $A$ and $B$ is 0, and the diodes $D_{aux1}$ and $D_{aux2}$ are conducting simultaneously. The capacitor $C_{B1}$ and inductor $L_{k1}$ begin to resonate. While the voltage $v_{BC}$ between point $B$ and $C$ is $+V_{in}$, and the current $i_{Lk2}$ begins to increases linearly. The currents are expressed as follows.

$$\begin{cases} i_{Lk1}(t) = \dfrac{-V_{in} - v_{CB1}(t_2)}{Z_{B1}}\sin\left(\omega_{B1}(t - t_2)\right) + i_{Lk1}(t_2)\cos\left(\omega_{B1}(t - t_2)\right) \\ i_{Lk2}(t) = i_{Lk2}(t_2) + \dfrac{V_{in} - n_{aux2}V_{aux2}}{L_{k2} + n_{aux2}^2 L_{f2}}(t - t_2) \end{cases} \tag{3}$$

*Interval 4 [$t_3 \le t < t_4$; see Fig. 3 (d)]:* This interval starts when switch $S_1$ turns off and switch $S_2$ turns on at $t_3$. The switch $S_3$ and $S_6$ has already conducted before $t_3$. The resonant currents $i_{Lr1}$, $i_{Lr2}$ and $i_{Lr3}$ vary in the sinusoidal waveform by resonance. The input voltages of resonant tank phase $A$ and $C$ are 0, while the input voltage of resonant tank phase $B$ is $+V_{in}$. The rectifier diodes $D_{o2}$, $D_{o3}$ and $D_{o6}$ conduct during this mode. And the magnetizing current $i_{Lm1}$ and $i_{Lm3}$ decrease linearly by the clamped voltage, while the magnetizing current $i_{Lm2}$ increases linearly. In the full bridge converters, the voltage $v_{AB}$ between point $A$ and $B$ is $-V_{in}$, and the current $i_{Lk1}$ begins to decreases linearly. The voltage $v_{BC}$ between point $B$ and $C$ is $+V_{in}$, and the current $i_{Lk2}$ goes on increasing linearly. The currents are expressed as follows.

$$\begin{cases} i_{Lk1}(t) = i_{Lk1}(t_3) + \dfrac{V_{in} - n_{aux1}V_{aux1}}{L_{k1} + n_{aux1}^2 L_{f1}}(t - t_3) \\ i_{Lk2}(t) = i_{Lk2}(t_3) + \dfrac{V_{in} - n_{aux2}V_{aux2}}{L_{k2} + n_{aux2}^2 L_{f2}}(t - t_3) \end{cases} \tag{4}$$

*Interval 5 [$t_4 \le t < t_5$; see Fig. 3 (e)]:* This interval starts when switch $S_6$ turns off and switch $S_5$ turns on at $t_4$. The switch $S_2$ and $S_3$ has already conducted before $t_4$. The resonant currents $i_{Lr1}$, $i_{Lr2}$ and $i_{Lr3}$ vary in the sinusoidal waveform by resonance. The input voltage of the resonant tank phase $A$ is 0, the input voltages of the resonant tank phase $B$ and phase $C$ are $+V_{in}$. The rectifier diodes $D_{o2}$, $D_{o3}$ and $D_{o5}$ are conducting. The magnetizing current $i_{Lm1}$ decreases linearly by the clamped voltage, while the magnetizing current $i_{Lm2}$ and $i_{Lm3}$

increase linearly. In the full bridge converters, the voltage $v_{AB}$ between point $A$ and $B$ $v_{AB}$ is $-V_{in}$, as a result, the current $i_{Lk1}$ decreases linearly. The voltage $v_{BC}$ between point $B$ and $C$ $v_{BC}$ is 0, and the rectifier diodes $D_{aux3}$ and $D_{aux4}$ are conducting simultaneously. The capacitor $C_{B2}$ and inductor $L_{k2}$ begin to resonate. The currents are expressed as follows.

$$\begin{cases} i_{Lk1}(t) = i_{Lk1}(t_4) + \dfrac{V_{in} - n_{aux1}V_{aux1}}{L_{k1} + n_{aux1}^2 L_{f1}}(t - t_4) \\ i_{Lk2}(t) = \dfrac{-V_{in} - v_{CB2}(t_4)}{Z_{B2}}\sin\left(\omega_{B2}(t - t_4)\right) + i_{Lk2}(t_4)\cos\left(\omega_{B2}(t - t_4)\right) \end{cases} \tag{5}$$

*Interval 6 [$t_5 \le t \le t_6$; see Fig. 3 (f)]:* This interval starts when switch $S_3$ turns off and $S_4$ turns on at $t_5$. The switch $S_2$ and $S_5$ has already conducted. The resonant currents $i_{Lr1}$, $i_{Lr2}$ and $i_{Lr3}$ vary in the sinusoidal waveform by resonance. The input voltages of the resonant tank phase $A$ and phase $B$ is 0, the input voltage of the resonant tank phase $C$ is $+V_{in}$. The rectifier diodes $D_{o2}$, $D_{o4}$ and $D_{o5}$ are conducting. The magnetizing current $i_{Lm1}$ goes on decreasing linearly, while the magnetizing current $i_{Lm2}$ begins to decrease linearly, and the magnetizing current $i_{Lm3}$ goes on increasing linearly. In the full bridge converters, the voltage $v_{AB}$ between point $A$ and $B$ $v_{AB}$ is 0, and the rectifier diodes $D_{aux1}$ and $D_{aux2}$ are conducting simultaneously. The capacitor $C_{B1}$ and inductor $L_{k1}$ begin to resonate. The voltage $v_{BC}$ between point $B$ and $C$ $v_{BC}$ is $-V_{in}$, and the current begins to decrease. The currents are expressed as follows.

$$\begin{cases} i_{Lk1}(t) = \dfrac{-V_{in} - v_{CB1}(t_5)}{Z_{B1}}\sin\left(\omega_{B1}(t - t_5)\right) + i_{Lk1}(t_5)\cos\left(\omega_{B1}(t - t_5)\right) \\ i_{Lk2}(t) = i_{Lk2}(t_5) + \dfrac{V_{in} - n_{aux2}V_{aux2}}{L_{k2} + n_{aux2}^2 L_{f2}}(t - t_5) \end{cases} \tag{6}$$

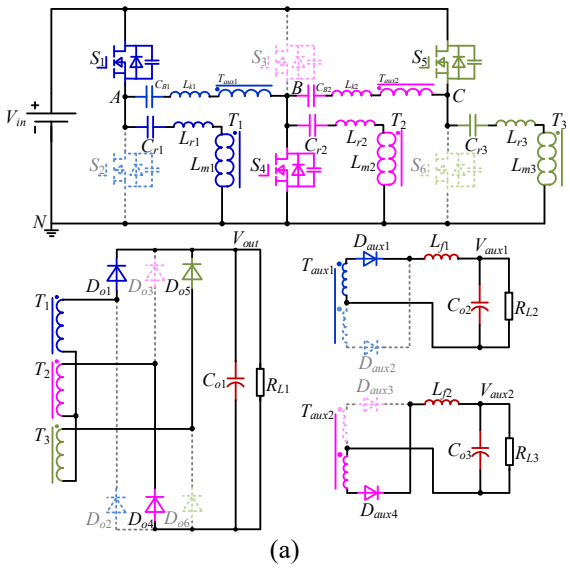

(a)

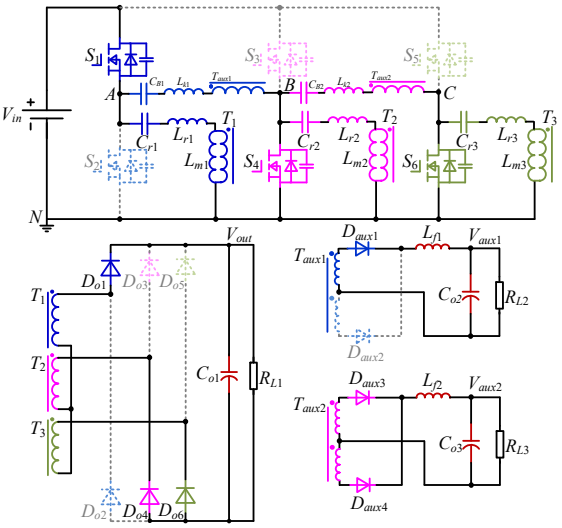

(b)

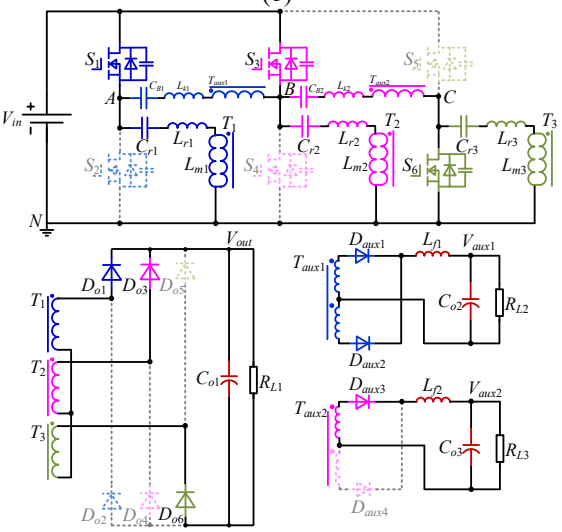

(c)

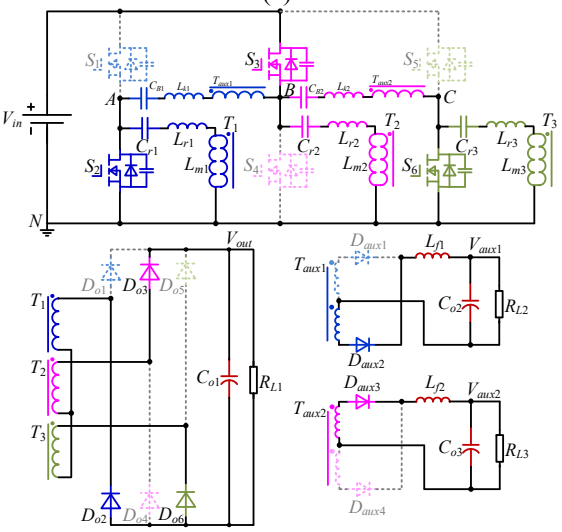

(d)

This article has been accepted for publication in a future issue of this journal, but has not been fully edited. Content may change prior to final publication. Citation information: DOI 10.1109/JESTPE.2021.3139905, IEEE Journal of Emerging and Selected Topics in Power Electronics



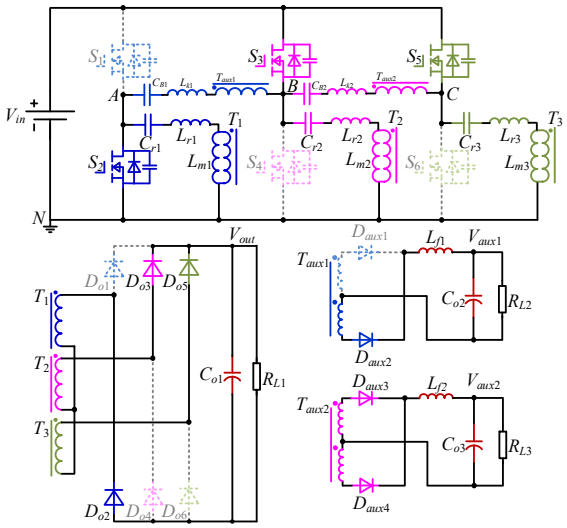

(e)

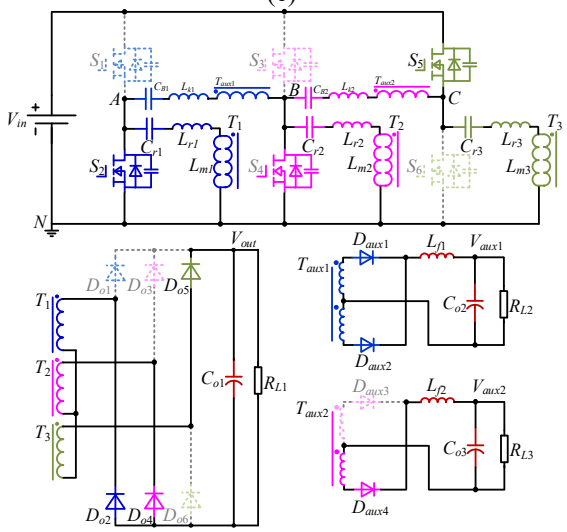

(f)

Fig. 3 Operational modes of the proposed converter, (a) Interval 1 ( $t_0 \le t < t_1$ ), (b) Interval 2 ( $t_1 \le t < t_2$ ), (c) Interval 3 ( $t_2 \le t < t_3$ ), (d) Interval 4 ( $t_3 \le t < t_4$ ), (e) Interval 5 ( $t_4 \le t < t_5$ ), (f) Interval 6 ( $t_5 \le t \le t_6$ ).

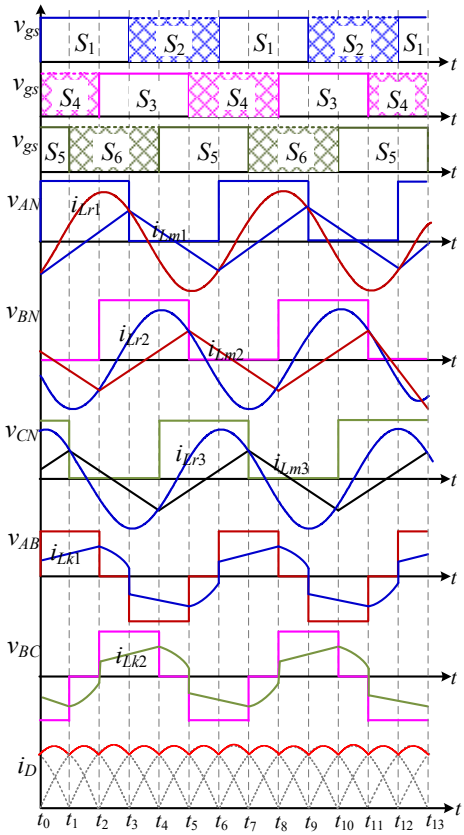

Fig. 4 Principal waveforms of the proposed converter.

## III. CHARACTERISTICS AND ANALYSIS

The proposed topology is derived from the integration of the three-phase LLC resonant converter and the full bridge converters. The multi outputs are regulated by the hybrid modulation of PFM and PWM without cross regulation. This section analyzes the characteristics of the three phase LLC resonant converter firstly, and then analyzes the characteristics of the full bridge converter. Finally, a design example is presented to illustrate the design procedure.

### *A. Characteristics Analysis of the Three-Phase Resonant Converter*

The converter is analyzed using the fundamental harmonic analysis (FHA). All the components are reflected to the primary side, and the circuit can be simplified into one-phase circuit, as shown in Fig. 5 (a), the per-phase phasor equivalent circuit can be depicted in Fig. 5 (b). The input voltage in Fig. 5 (b) is represented by the fundamental component of the square-wave voltage across *AN*, the equivalent output resistance can be derived as [33].

$$R_{ac} = \frac{8n^2}{\pi^2} R_L \tag{7}$$

This article has been accepted for publication in a future issue of this journal, but has not been fully edited. Content may change prior to final publication. Citation information: DOI 10.1109/JESTPE.2021.3139905, IEEE Journal of Emerging and Selected Topics in Power Electronics



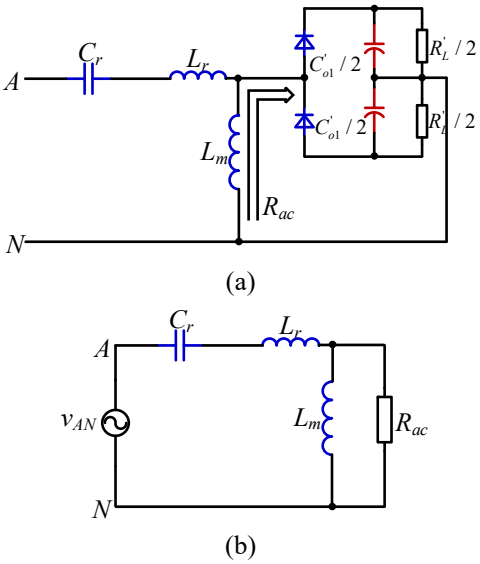


Fig. 5 Equivalent single-phase circuit by fundamental harmonic analysis, (a) equivalent circuit of one phase, (b) per-phase phasor equivalent circuit.

Based on the FHA, the voltage gain of the per-phase LLC resonant circuit can be express as follow.

$$M_H = \frac{1}{n}\frac{1}{\sqrt{\left(1+k-\frac{k}{f_n^2}\right)^2+Q^2\left(f_n-\frac{1}{f_n}\right)^2}} \tag{8}$$

Where $k$ is the inductance ratio, $f_n$ is normalized frequency, and $Q$ is quality factor, which are defined as follows.

$$k=\frac{L_r}{L_m} \qquad f_n=\frac{f_s}{f_r} \qquad Q=\frac{\sqrt{L_r/C_r}}{R_{ac}} \tag{9}$$

Where $f_s$ is the switching frequency, and $f_r$ is the resonant frequency of resonant inductor $L_r$ and resonant capacitor $C_r$.

### *B. Characteristic Analysis of the full bridge Converter*

The two auxiliary output voltages $V_{aux1}$ and $V_{aux2}$ are the output voltage of two full bridge converters who share one bridge branch. In the conventional design of the full bridge converter, the auxiliary inductor needs to be specially designed to help achieving soft-switching operation. However, the auxiliary inductor will cause the duty cycle loss, and the bigger the more serious. Therefore, there is a balance between the soft-switching operation and the duty cycle loss in the conventional full bridge converter. What's worse, the soft-switching operation will lose under light load condition, which will decrease the reliability and efficiency.

In the proposed multi-outputs converter, the power switches can keep the soft-switching operation within the entire load range by the existence of the LLC resonant tank in the proposed converter. As a consequence, the auxiliary inductor in the proposed converter does not need to be specially designed. As a consequence, the duty cycle loss caused by the auxiliary inductor can be ignored. In this paper, the auxiliary inductors $L_{k1}$ and $L_{k2}$ are the leakage inductance of the transformer $T_{aux1}$ and $T_{aux2}$. The voltage gain of the full bridge phase shift converter can be expressed as follows without considering the duty cycle loss.

$$M_L=\frac{\varphi}{\pi n_{aux}} \tag{10}$$

Where $n_{aux}$ is turns ratio of the transformer, and the phase shift angle $\varphi$ in (10) is 120° in the three-phase LLC resonant converter.

From the above analysis, the PFM is adopted in the LLC resonant converter and the PWM is adopted in the full bridge converter. The multi output voltages of the LLC resonant converter and the full bridge converter are regulated by different categories of variables, which will not affect each other.

### *C. Design Considerations*

A design example is presented to illustrate the design procedure. The proposed converter is designed and built according to the following key specifications.

Input voltage $V_{in}$: 400 $V_{DC}$
Main output voltage $V_{out}$: 200V-400 $V_{DC}$
Auxiliary output voltage $V_{aux1}$: 36 $V_{DC}$
Auxiliary output voltage $V_{aux2}$: 48 $V_{DC}$
Maximum output power of main output voltage $P_{out}$: 1kW
Maximum output power of auxiliary output power $P_{aux1}$ and $P_{aux2}$: $P_{aux1}$=200W, $P_{aux2}$=200W

#### *1). Selection of the Resonant Tank Components*

To determine the values of the resonant tank components, it is necessary to select the turns ratio of the transformer firstly. The turns ratio is determined that the efficiency of the converter in the mid-voltage (300V) is maximized since the converter is expected to work at the mid-voltage most of time. The voltage gain of the three-phase LLC resonant is expressed in (10), for the prototype circuit, turns ratio is determined by assuming that the converter operates with voltage gain $M_H$=1, so that the turns ratio can be calculated as follows.

$$n=\frac{V_{in}}{V_{out}}=1\times\frac{400}{300}\approx 1.5 \tag{11}$$

The turns ratio $n$ is determined to be 1.5. The maximum voltage gain $M_{H\_max}=V_{out\_max}/V_{in}$=1, and the minimum voltage gain $M_{H\_min}=V_{out\_min}/V_{in}$=0.5.

The resonant frequency $f_r$ is determined to be 100kHz in the prototype circuit, and the resonant circuit's parameters can be calculated at full load.

$$\begin{aligned} C_r &= \frac{1}{2\pi\times Q\times f_r\times R_{ac}} \\ &= \frac{1}{2\pi\times 0.45\times 100\times 10^3\times 73}=48.4nF \Rightarrow 47nF \end{aligned} \tag{12}$$

Where $Q$ is load factor, whose value is usually selected ranging from 0.3 to 0.5 when determining the circuit parameters. $R_{ac}$ is equivalent load resistance which can be calculated as follows.

$$R_{ac}=\frac{8\times n^2}{\pi^2}\times\frac{V_{out}}{I_{out}}=\frac{8\times 1.5^2}{\pi^2}\times\frac{200}{5}=73\Omega \tag{13}$$

The resonant capacitor $C_r$ is determined to be 47nF. The resonant inductor $L_r$ can be determined as follows.

This article has been accepted for publication in a future issue of this journal, but has not been fully edited. Content may change prior to final publication. Citation information: DOI 10.1109/JESTPE.2021.3139905, IEEE Journal of Emerging and Selected Topics in Power Electronics



$$L_r = \frac{1}{(2\pi \times f_r)^2 C_r} = \frac{1}{\left(2\pi \times 100 \times 10^3\right)^2 \times 47 \times 10^{-9}} = 53\mu H \quad (14)$$

The resonant inductor $L_r$ is determined to be 53μH.

*2). Selection of Components of Full Bridge Converter*

The power switches in the proposed converter can keep ZVS within the entire load range by the existence of the three-phase LLC resonant tank. The inductor in the full bridge converter doesn't need to be specially designed, and the only component needs to determine is the turns ratio of the transformer. The voltage gain of the full bridge converter is expressed in (10) and the phase shift angle $\varphi$ is 120°, and the turns ratio of the transformer is determined as follows.

$$n_{aux} = \frac{V_{in}}{V_{aux}} \times \frac{120}{180} \quad (15)$$

The turns ratio $n_{aux1}$ of transformer $T_{aux1}$ is determined to be 7.4 and the turns ratio $n_{aux2}$ of transformer $T_{aux2}$ is determined to be 5.6. The key parameters used in the prototype circuit are summarized in Table 1.

## IV. SIMULATION AND EXPERIMENTAL VERIFICATIONS

### *A. Simulation Results*

*1). Steady state waveforms*

A MATLA/Simulink simulation model used to verify the analysis of the proposed multi-outputs topology is built and simulated. The key parameters used in the simulation model is listed in Table 1. Fig. 6 shows the simulated waveforms of the proposed converter under $V_{out}$=300V, $V_{aux1}$=36V, $V_{aux2}$=48V with full load. Fig. 6 (a) shows the simulated resonant currents of the three-phase resonant tank that varies in the sinusoidal shape. Fig. 6 (b) shows the primary side currents of the full bridge converter. Fig. 6 (c) shows the switching current flowing through the power switch, and it is demonstrated that zero voltage turn on can be achieved on the power switches.

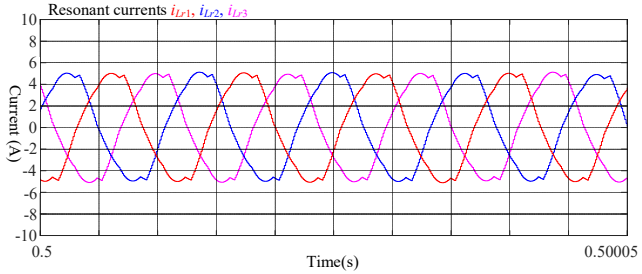


(a)

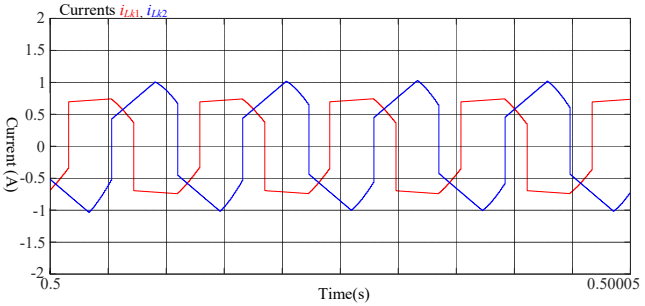


(b)

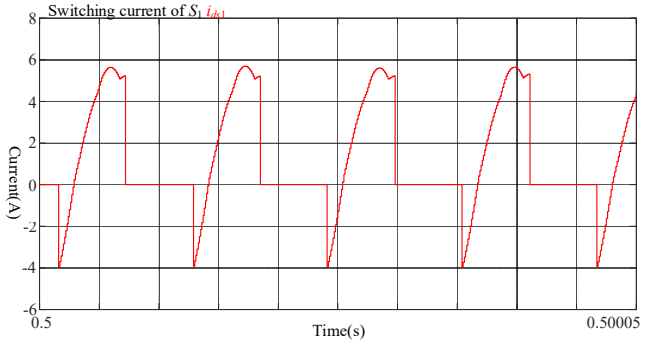


(c)

Fig. 6 Simulated waveforms of proposed multi-outputs converter at $V_{out}$=300V, $V_{aux1}$=36V, $V_{aux2}$=48V with full load. (a) Resonant currents of the three-phase resonant tank, (b) currents of the full bridge converter, (c) switching current of the power switch $S_1$.

*2). Transient waveforms*

Fig. 7 presents transient waveforms with load changes. Fig. 7 (a), (b) and (c) shows the transient waveforms with one of output powers of switches from half power to full power, while the other two output power remains unchanged. It can be seen that the variation of one of the outputs will not affect the other two outputs.

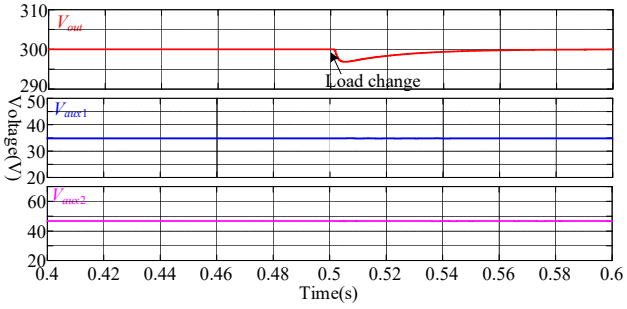


(a)

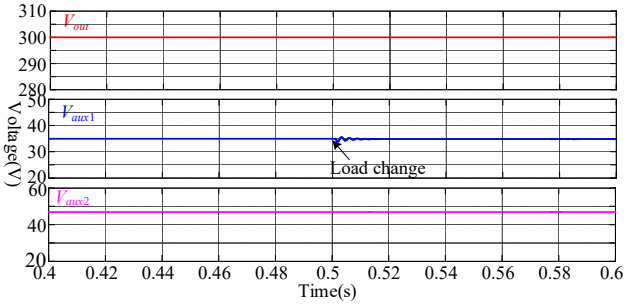


(b)

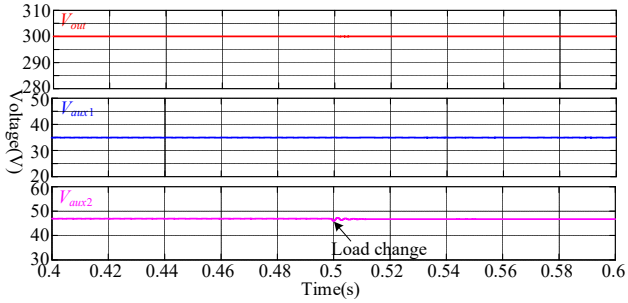


(c)

Fig. 7 Transient waveforms ($V_{out}$=300V, $V_{aux1}$=36V, $V_{aux2}$=48V). (a) $P_{out}$ switches from half power to full power with $P_{aux1}$ and $P_{aux2}$ remain unchanged, (b) $P_{aux1}$ switches from half power to full power with $P_{out}$ and $P_{aux2}$ remain unchanged, (c) $P_{aux2}$ switches from half power to full power with $P_{out}$ and $P_{aux1}$ remain unchanged.

*B. Experimental Results and Analysis*

A 1.4kW MOSFET-based prototype is built to verify the feasibility and effectiveness of the proposed converter, and the experimental prototype is DSP controlled with key circuit parameters listed in Table 1. The inductor $L_{k1}$ and $L_{k2}$ are the leakage inductance of transformer of $T_{aux1}$ and $T_{aux2}$, respectively. The full bridge converters are designed to be operated at continuous conduction mode, and the phase shift angles $\varphi_1$ and $\varphi_2$ between the two half bridge branches are 120°. Fig. 8 shows the key circuit parameters utilized in the experimental prototypes. TMS320F28335 is used as the microcontroller to control the power circuit, and the parameters of the power circuits utilized in the experimental prototype are listed in Table 1. The experimental platform is shown in Fig. 8, a programmable DC voltage source (from Chroma) is used as the input voltage, and two DC electric loads are used as the load for the multi outputs. One DC electric load (from ITECH) is used as the load for the main output $V_{out}$, the other DC electric load (from Chroma) which has four isolated channels and two channels are used as the loads for the auxiliary outputs $V_{aux1}$ and $V_{aux2}$. And oscilloscopes are used to observe the experimental waveforms.

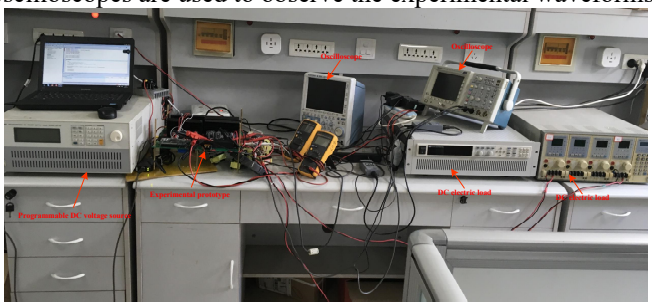


Fig. 8 Experimental platform of the proposed converter.

The maximum output power of the experimental prototype is 1.4kW, and the output power of $V_{out}$ is 1kW, while the output power of $V_{aux1}$ and $V_{aux2}$ is 200W. The output voltage $V_{out}$ is modulated by the switching frequency, which is ranged from 200V to 400V. The output voltages $V_{aux1}$ and $V_{aux2}$ are related to the phase shift angles between the three-phase interleaved bridge branches and the turns ratio of the transformers, and $V_{aux1}$ and $V_{aux2}$ are designed to be 36V and 48V.

Table 1 Key circuit parameters utilized in the experimental prototype.

| Components | Parameters |
|---|---|
| Circuit parameters for the output voltage $V_{out}$ | |
| $V_{in}$ (Input voltage) | 400V |
| $V_{out}$ (Output voltage) | 200V-400V |
| $P_{out}$ (Rated output power) | 1kW |
| $f_r$ (Resonant frequency) | 100kHz |
| $L_{r1}$=$L_{r2}$=$L_{r3}$ (Resonant inductor) | 53μH |
| $C_{r1}$=$C_{r2}$=$C_{r3}$ (Resonant capacitor) | 47nF |
| $L_{m1}$=$L_{m2}$=$L_{m3}$ (Magnetizing inductor) | 120μH |
| $n_1$=$n_2$=$n_3$ (Turns ratio of transformer) | 1.5 |
| $C_{o1}$ (Output filter capacitor) | 390μF/450V |
| $S_1$-$S_6$ (Power MOSFETs) | IPW65R080CFD |
| $D_{o1}$-$D_{o6}$ (Diodes) | FDCY25S65 |
| Deadtime | 400ns |
| Circuit parameters for the output voltage $V_{aux1}$ | |
| $V_{aux1}$ (Output voltage) | 36V |
| $P_{aux1}$ (Rated output power) | 200W |
| $L_{k1}$ (Leakage inductance) | 10μH |
| $C_{B1}$ (DC blocking capacitor) | 1μF |
| $n_{aux1}$ (Turns ratio of transformer) | 7.4 |
| $L_{f1}$ (Output filter inductor) | 200μH |
| $C_{o2}$ (Output filter capacitor) | 3000μF |
| $D_{aux1}$-$D_{aux2}$ (Diodes) | MBRF10H150CTG |
| Circuit parameters for the output voltage $V_{aux2}$ | |
| $V_{aux2}$ (Output voltage) | 48V |
| $P_{aux2}$ (Rated output power) | 200W |
| $L_{k2}$ (Leakage inductance) | 8μH |
| $C_{B2}$ (DC blocking capacitor) | 1μF |
| $n_{aux2}$ (Turns ratio of transformer) | 5.6 |
| $L_{f2}$ (Output filter inductor) | 200μH |
| $C_{o3}$ (Output filter capacitor) | 3000μF |
| $D_{aux3}$-$D_{aux4}$ (Diodes) | MBRF10H150CTG |

*1). Steady state waveforms*

The experimental results of the proposed multi-outputs converter are shown as follows. Fig. 9 shows the measured waveforms under $V_{out}$=300V, $V_{aux1}$=36V and $V_{aux2}$=48V with full load. The switching frequency of the power switches is near the resonant frequency. The measured currents of the full bridge converters are presented in Fig. 9 (a) and (b), and the resonant currents of the three-phase resonant tank are shown in Fig. 9 (c), and the triple output voltages $V_{out}$, $V_{aux1}$ and $V_{aux2}$ are demonstrated in Fig. 9 (d). Fig. 10 shows the measured waveforms under $V_{out}$=400V, $V_{aux1}$=36V and $V_{aux2}$=48V with full load. The switching frequency is below the resonant frequency. The measured currents of the full bridge converters

This article has been accepted for publication in a future issue of this journal, but has not been fully edited. Content may change prior to final publication. Citation information: DOI 10.1109/JESTPE.2021.3139905, IEEE Journal of Emerging and Selected Topics in Power Electronics



are presented in Fig. 10 (a) and (b). The measured resonant currents of the three-phase resonant tank are presented in Fig. 10 (c), and the triple output voltages $V_{out}$, $V_{aux1}$ and $V_{aux2}$ are demonstrated in Fig. 10 (d). It can be proved from the experimental results that the resonant currents vary in the sinusoidal waveform just as the theoretical analysis. The currents of the full bridge converters increase/decrease linearly as the input voltage is $+V_{in}$/$-V_{in}$, while during the input voltage is 0, the leakage inductance of the transformer $T_4$/$T_5$ begins to resonate with the dc-blocking capacitor $C_{B1}$/$C_{B2}$.

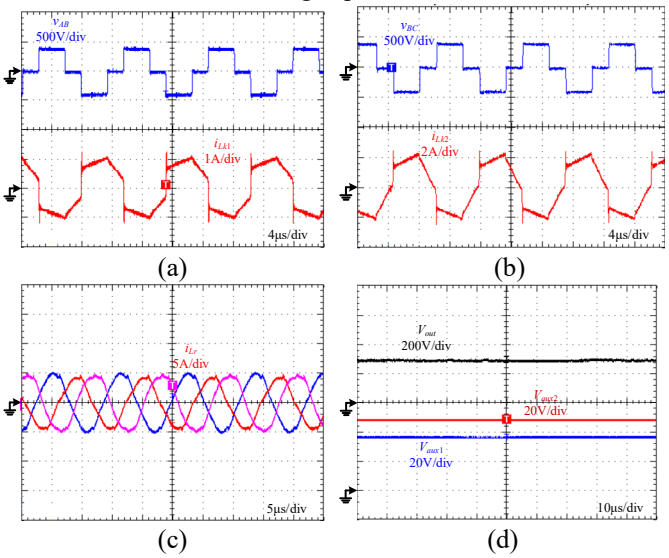


Fig. 9 Experimental waveforms at $V_{out}$=300V, $V_{aux1}$=36V, $V_{aux2}$=48V with full load. (a) Measured current waveforms of the full bridge converter $V_{aux1}$, (b) Measured current waveforms of the full bridge converter $V_{aux2}$, (c) Resonant currents of the three-phase resonant tank $i_{Lr1}$, $i_{Lr2}$ and $i_{Lr3}$, (d) Measured output voltages $V_{out}$, $V_{aux1}$ and $V_{aux2}$.

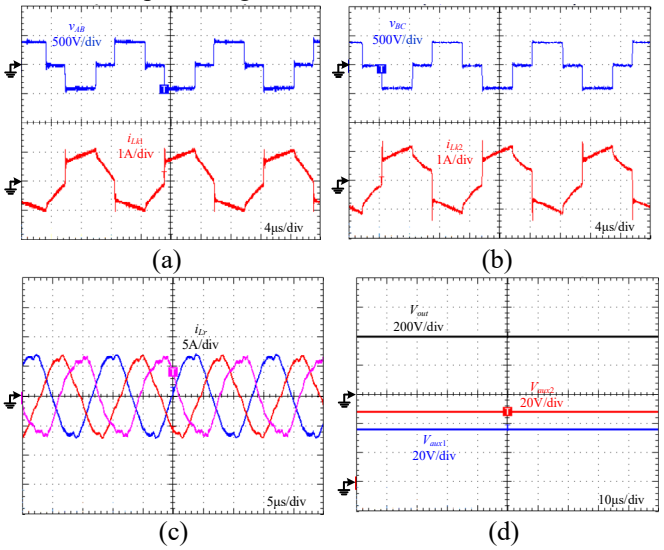


Fig. 10 Experimental waveforms at $V_{out}$=400V, $V_{aux1}$=36V, $V_{aux2}$=48V with full load. (a) Measured current waveforms of the full bridge converter $V_{aux1}$, (b) Measured current waveforms of the full bridge converter $V_{aux2}$, (c) Resonant currents of the three-phase resonant tank $i_{Lr1}$, $i_{Lr2}$ and $i_{Lr3}$, (d) Measured output voltages $V_{out}$, $V_{aux1}$ and $V_{aux2}$.

Fig. 11 shows the switching voltage and gate-driving signal of one of the power switches ($S_1$) under full power, it can be found that the switching voltage $V_{ds}$ falls down to zero before the gate-driving signal $V_{gs}$ turns on the power switch, which demonstrates that the ZVS operation can be ensured.

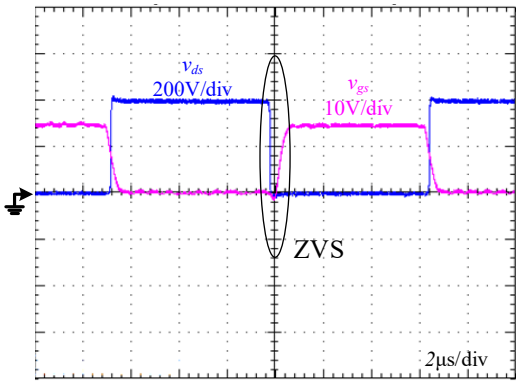


Fig. 11 Switching voltage and gate-driving signal, time scale: 2μs/div.

*2). Transient waveforms*

In order to prove the proposed multi outputs are free from cross regulation, transient experiment with load change is carried out. The load transient response waveforms are presented in Fig. 12. In order to present the variations of the output voltages during the transient response clearly, ac coupling of the output voltages is used. In Fig. 12 (a), $P_{aux1}$ and $P_{aux2}$ remain at full power unchanged, while $P_{out}$ switches from half power to full power. In Fig. 12 (b), $P_{out}$ and $P_{aux2}$ remain at full power unchanged, while $P_{aux1}$ switches from full power to half power. It can be found that the variation of one voltage will not affect the other two voltages. It can be demonstrated that the triple output voltages do not affect each other, and the triple outputs are free from cross regulation.

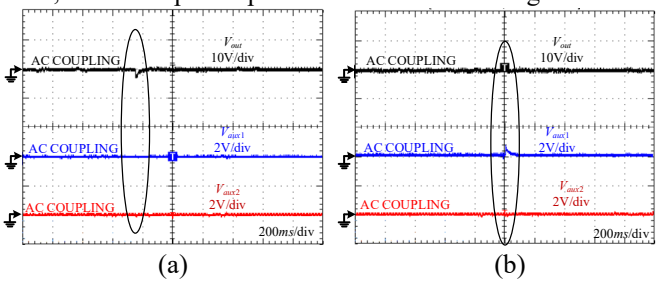


Fig. 12 Measured load transient waveforms: $P_{aux1}$ switches from half power to full power with $P_{out}$ and $P_{aux2}$ remain unchanged, time scale: 200ms/div.

*3). Measured efficiency*

Fig. 13, Fig. 14 and Fig. 15 show the measured efficiency curve. In Fig. 13, $P_{aux1}$ and $P_{aux2}$ keep at full power unchanged, while the efficiency of the experimental prototype is measured as $P_{out}$ varies from 10% power to full power under different output voltages. The measured minimum efficiency of the prototype is 88.1% at 400V 10% power, and the measured maximum efficiency is 95.6% at 200V 70% power. In Fig. 14, $P_{out}$ and $P_{aux2}$ keep at full power unchanged, while the efficiency is measured as $P_{aux1}$ varies from 10% power to full power under different $V_{out}$. In Fig. 15, $P_{out}$ and $P_{aux1}$ keep at full power unchanged, while the efficiency is measured as $P_{aux2}$ varies from 10% load to full power under different $V_{out}$. As shown in Fig. 14 and Fig. 15, it is depicted that the

This article has been accepted for publication in a future issue of this journal, but has not been fully edited. Content may change prior to final publication. Citation information: DOI 10.1109/JESTPE.2021.3139905, IEEE Journal of Emerging and Selected Topics in Power Electronics



efficiencies change a little while the power of $P_{out}$ keeps unchanged. This is mainly because most of the power losses come from the three-phase resonant converter.

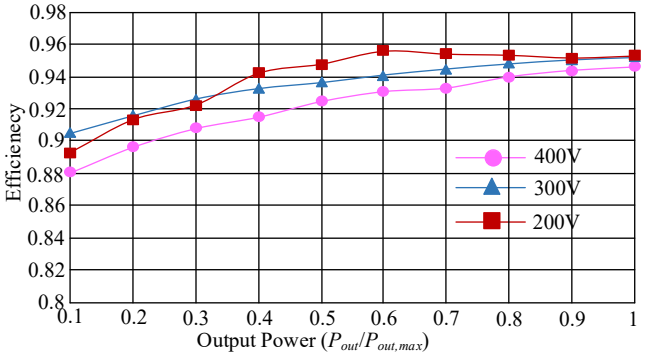


Fig. 13 Efficiency *vs* Output power ($P_{aux1}$=200W, $P_{aux2}$=200W).

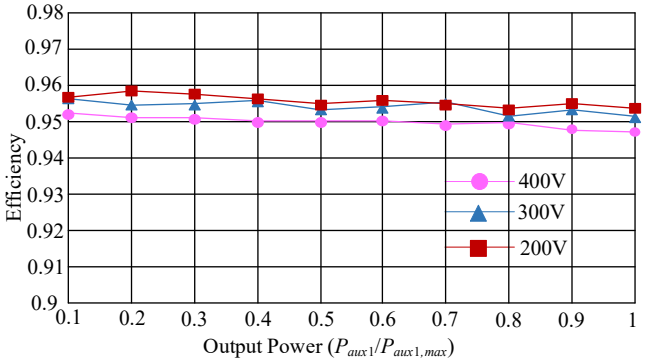


Fig. 14 Efficiency *vs* Output Power ($P_{out}$=1kW, $P_{aux2}$=200W).

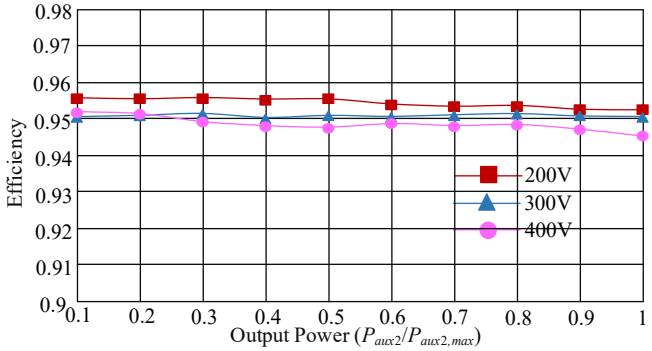


Fig. 15 Efficiency *vs* Output power ($P_{out}$=1kW, $P_{au1}$=200W).

### *C. Power Loss Analysis*

A breakdown of the power loss incurred at 1.4kW with $V_{out}$=300V, $V_{aux1}$=36V, $V_{aux2}$=48V is shown in Fig. 16. The power loss calculation is based on a combination of experimental results (like RMS currents of the resonant current) and theoretical data from datasheet (like $R_{ds(on)}$ of the MOSFETs and forward voltage drop $V_F$ of the diodes) and the calculation method is based on the loss calculation method in [34,35]. The power loss includes: the switching and conduction loss of the MOFETs, the conduction loss of diodes, the loss of inductors and the loss of transformers. In Fig. 16, the subscript "sw" and "con" represents the switching loss and conduction loss, respectively. The MOSFETs can achieve ZVS, so there is only turn off loss. The diodes can achieve ZCS, so there is no switching loss of diodes. The subscript "Cu" and "Fe" represent the winding loss and core loss of the magnetic components. Since the series resistance of the output capacitor is very small, the power loss of the output capacitor is ignored. From the results, it can be found that almost 54.7% of the total loss can be attributed to magnetic loss by transformers and inductors. 4.24% is switching loss as the soft-switching operation can be achieved on the power switches. By further investigating the power loss chart, the efficiency can be improved by increasing the switching frequency. By increasing the switching frequency, fewer winding turns and lower core loss are expected. Therefore, the efficiency of the converter can be improved furtherly.

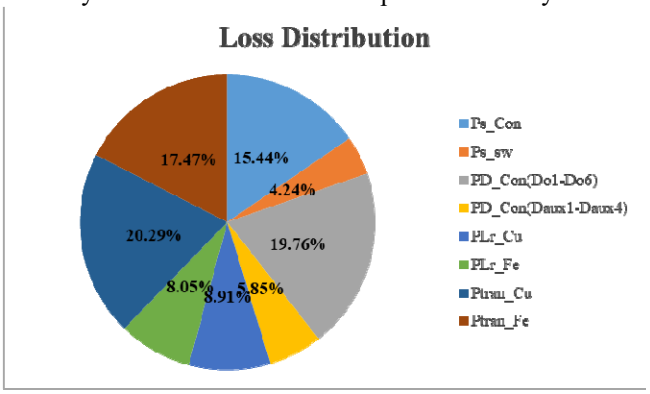


Fig. 16 Estimated loss distribution under $V_{out}$=300V, $V_{aux1}$=36V, $V_{aux2}$=48V with full load (Total loss=70.74W).

## V. Conclusion

The proposed multi-outputs DC-DC topology is derived from the hybrid modulated of three-phase LLC resonant converter and the full bridge converter. With the hybrid modulation of PWM and PFM, the multi outputs of the proposed converter are controlled and free from cross regulation. In addition, the multi outputs are isolated from each other by the high frequency transformer. The power level of the auxiliary output voltages could be high. In the designed prototype circuit, the output power of the auxiliary output voltages is about two-thirds of the per-phase resonant tank of the main output voltage, while the power switches still can keep zero voltage turn on. The three-phase LLC resonant tank can reduce the resonant current and thus increase the system efficiency. Moreover, the power switches on the primary side can keep ZVS within the full load range. The proposed topology shows features of reduced number of power switches, higher power density. In consequence, all of the advantages of the proposed converter will lead to a compact, efficient and cost-effective design. Finally, experimental results have validated the feasibility and effectiveness of the proposed converter.

## References

[1] M. Yilmaz, P. T. Krein, "Review of Battery Charger Topologies, Charging Power Levels, and Infrastructure for Plug-In Electric and Hybrid Vehicles," *IEEE Trans. Power Electron.*, vol. 28, no. 5, pp. 2151-2169, May 2013.

[2] G. Chen, Y. Deng, J. Dong, Y. Hu, L. Jiang, X. He, "Integrated Multiple-Output Synchronous Buck Converter for Electric Vehicle Power Supply," *IEEE Trans. Veh. Technol.*, vol. 66, no. 7, pp. 5752-5761, Jul. 2017.

[3] X. Gao, H. Wu, Y. Xing, "A Multioutput LLC Resonant Converter With Semi-Active Rectifiers," *IEEE J. Emerging Sel. Top. Power Electron.*, vol. 5, no. 4, pp. 1819-1827, Dec. 2017.

[4] G. Chen, Z. Jin, Y. Liu, Y. Hu, J. Zhang, X. Qing, "Programmable Topology Derivation and Analysis of Integrated Three-Port DC-DC Converters with Reduced Switches for Low-Cost Applications," *IEEE Trans. Ind. Electron.*, vol. 66, no. 9, pp. 6649-6660, Sept. 2019.

[5] G. Lu, P. Zhang, "A Novel Leakage-Current-Based Online Insulation Monitoring Strategy for Converter Transformers Using Common-Mode and Differential-Mode Harmonics in VSC System," *IEEE Trans. Ind. Electron.*, vol. 68, no. 2, pp. 1636-1645, Feb. 2021.

[6] G. Yang, F. Xiao, X. Fan, R. Wang, J. Liu, "Three-Phase Three-Level Phase Shifted PWM DC-DC Converter for Electric Ship MVDC Application," *IEEE J. Emerging Sel. Top. Power Electron.*, vol. 5, no. 1, pp. 162-170, Mar. 2017.

[7] N. Shafiei, M. Ordonez, "Improving the Regulation Range of EV Battery Chargers With L3C2 Resonant Converters," *IEEE Trans. Power Electron.*, vol. 30, no. 6, pp. 3166-3184, Jun. 2015.

[8] F. C. Lee, Q. Li, A. Nabih, "High Frequency Resonant Converters: An Overview on the Magnetic Design and Control Methods," *IEEE J. Emerging Sel. Top. Power Electron.*, vol. 9, no. 1, pp. 11-23, Feb. 2021.

[9] L. Zhao, H. Li, X. Wu, J. Zhang, "An Improved Phase-Shifted Full-Bridge Converter with Wide-Range ZVS and Reduced Filter Requirement," *IEEE Trans. Ind. Electron.*, vol. 65, no. 3, pp. 2167-2176, Mar. 2018.

[10] G. D. Capua, S. A. Shirsavar, M. A. Hallworth, N. Femia, "An Enhanced Model for Small-Signal Analysis of the Phase-Shifted Full-Bridge Converter," *IEEE Trans. Power Electron.*, vol. 30, no. 3, pp. 1567-1576, Mar. 2015.

[11] L. Zhao, H. Li, Y. Hou, Y. Yu, "Operation Analysis of A Phase-Sifted Full-Bridge Converter During the Dead-Time Interval," *IET Power Electron.*, vol. 29, no. 9, pp. 1777-1783, 2016.

[12] J. Zhu, Q. Qian, S. Lu, W. Sun, H. Tian, "A Phase-shift Triple Full-Bridge Converter with Three Shared Leading-legs," *IEEE J. Emerging Sel. Top. Power Electron.*, vol. 6, no. 4, pp. 1912-1920, Dec. 2018.

[13] II. O. Lee, "Hybrid PWM-Resonant Converter for Electric Vehicle On-Board Battery Chargers," *IEEE Trans. Power Electron.*, vol. 31, no. 5, pp. 3639-3649, May 2016.

[14] B. Gu, J. S. Lai , N. Kees, C. Zheng, "Hybrid-Switching Full-Bridge DC–DC Converter With Minimal Voltage Stress of Bridge Rectifier, Reduced Circulating Losses, and Filter Requirement for Electric Vehicle Battery Chargers," *IEEE Trans. Power Electron.*, vol. 28, no. 3, pp. 1132-1144, Mar. 2013.

[15] J. Liu, J. Zhang, T. O. Zheng, J. Yang, "A Modified Gain Model and the Corresponding Design Method for an LLC Resonant Converter," *IEEE Trans. Power Electron.*, vol. 32, no. 9, pp. 6716-6727, Sep. 2017.

[16] H. Vu, W. Choi, "A Novel Dual Full-Bridge LLC Resonant Converter for CC and CV Charges of Batteries for Electric Vehicles," *IEEE Trans. Ind. Electron.*, vol. 65, no. 3, pp. 2212-2225, Mar. 2018.

[17] F. Musavi, M. Cracium, D. S. Cautam, W. Eberle, "Control Strategies for Wide Output Voltage Range LLC Resonant DC–DC Converters in Battery Chargers," *IEEE Trans. Veh. Technol.*, vol. 63, no. 3, pp. 1117-1125, Mar. 2014.

[18] J. Deng, C. C. Mi, R. Ma, S. Li, "Design of LLC Resonant Converters Based on Operation-Mode Analysis for Level Two PHEV Battery Chargers," *IEEE/ASME Trans. Mechatron.*, vol. 20, no. 4, pp. 1595-1606, Aug. 2015.

[19] H. Wang, S. Dusmez, A. Khaligh, "Design and Analysis of a Full-Bridge LLC-Based PEV Charger Optimized for Wide Battery Voltage Range," *IEEE Trans. Veh. Technol.*, vol. 63, no. 4, pp. 1603-1613, May 2014.

[20] Z. Hu, Y. Qiu, L. Wang, Y. Liu, "An Interleaved LLC Resonant Converter Operating at Constant Switching Frequency," *IEEE Trans. Power Electron.*, vol. 29, no. 6, pp. 2931-2943, Jun. 2016.

[21] K. Murata, F. Kurokawa, "An Interleaved PFM LLC Resonant Converter With Phase-Shift Compensation," *IEEE Trans. Power Electron.*, vol. 31, no. 3, pp. 2264-2272, Mar. 2016.

[22] Z. Hu, Y. Qiu, Y. Liu, P. C. Sen, "A Control Strategy and Design Method for Interleaved LLC Converters Operating at Variable Switching Frequency," *IEEE Trans. Power Electron.*, vol. 29, no. 8, pp. 4426-4437, Aug. 2014.

[23] D. Moon, J. Park, S. Choi, "New Interleaved Current-Fed Resonant Converter With Significantly Reduced High Current Side Output Filter for EV and HEV Applications," *IEEE Trans. Power Electron.*, vol. 30, no. 8, pp. 4264-4271, Aug. 2015.

[24] S. Kim, J. W. Baek, M. H. Ryu, J. H. Kim, J. H. Jung, "The High-Efficiency Isolated AC–DC Converter Using the Three-Phase Interleaved LLC Resonant Converter Employing the Y-Connected Rectifier," *IEEE Trans. Power Electron.*, vol. 29, no. 8, pp. 4017-4028, Aug. 2014.

[25] Wang, Y. Chen, Y. Liu, J. Afsharian, Z. Yang, "A Passive Current Sharing Method with Common Inductor Multiphase LLC Resonant Converter," *IEEE Trans. Power Electron.*, vol. 32, no. 9, pp. 6994-7010, Sep. 2017.

[26] M. Kobayashi, M. Yamamoto, "Current Balance Performance Evaluations for Transformer-Linked Three Phase DC-DC LLC Resonant Converter," in *Proc. 2012 International Conference on Renewable Energy Research and Applications (ICRERA)*, pp. 1-3, 2012.

[27] Y. Nakakohara, H. Otake, T. M. Evans, T. Yoshida, M. Tsuruya, K. Nakahara, "Three Phase LLC Series Resonant DC/DC Converter Using SiC MOSFETs to Realize High Voltage and High Frequency Operation," *IEEE Trans. Ind. Electron.*, vol. 63, no. 4, pp. 2103-2110, Apr. 2016.

[28] S. H. Ahn, S. R. Jang, H. Ryoo, "High-efficiency Bidirectional Three-phase LCC Resonant Converter with a Wide Load Range," *IEEE Trans. Power Electron.*, vol. 34, no. 1, pp. 97-105, Jan. 2019.

[29] C. Fei, R. Gadelrab, Q. Li, F. C. Lee, "High-Frequency Three-Phase Interleaved LLC Resonant Converter With GaN Devices and Integrated Planar Magnetics," *IEEE J. Emerging Sel. Top. Power Electron.*, vol. 7, no. 2, pp. 653-663, Jun. 2019.

[30] E. Orietti, P. Mattavelli, G. Spiazzi, "Current Sharing in Three-Phase LLC Interleaved Resonant Converter," in *Proc. 2009 IEEE Energy Conversion Congress and Exposition*, pp. 1-8, 2009.

[31] M. B. F. Prieto, S. P. Litran, E. D. Aranda, J. M. E. Gomez, "New Single-Input, Multiple-Output Converter Topologies: Combining Single-Switch Nonisolated dc-dc Converters for Single-Input, Multiple-Output Applications," *IEEE Ind. Electron. Mag.*, vol. 10, no. 2, pp. 6-20, Jun. 2016.

[32] Z. Li, S. Dusmez, H. Wang, "A Novel Soft-Switching Secondary-Side Modulated Multi-output DC/DC Converter with Extended ZVS Range," *IEEE Trans. Power Electron.*, vol. 34, no. 1, pp. 106-116, Jan. 2019.

[33] M.S. Almardy, A.K.S. Bhat, "Three-Phase (LC)(L)-Type Series-Resonant Converter With Capacitive Output Filter," *IEEE Trans. Power Electron.*, vol. 26, no. 4, pp. 1172-1183, Apr. 2011.

[34] C. Li, D. Xu, "Family of Enhanced ZCS Single-Stage Single-Phase Isolated AC–DC Converter for High-Power High-Voltage DC Supply," *IEEE Trans. Ind. Electron.*, vol. 64, no. 5, pp. 3629-3639, May 2017.

[35] C. Li, Y. Zhang, Z. Cao, D. Xu, "Single-Phase Single-Stage Isolated ZCS Current-Fed Full-Bridge Converter for High-Power AC/DC Applications," *IEEE Trans. Power Electron.*, vol. 32, no. 9, pp.6800-6812, Sep. 2017.

**Guangdi Li** received the B.E.E degree from the College of Information Science and Engineering, Northeastern University, Shenyang, China, in 2013, and the Ph.D. degree in power electronics and electric drive from the College of Electrical Engineering, Zhejiang University, in 2020.

He is currently a Postdoctoral Researcher with the College of College of Information Science and Engineering, Northeastern University, Shenyang, China. His current research interests include resonant DC-DC converters, control and modeling of grid-connected converters. He has published more than 10 SCI or EI indexed papers. He is a member of IEEE PES Intelligent Grid & Emerging Technologies Satellite Committee – China. He is currently a member of IEEE. He is also an active reviewer of some peer reviewed journals and international conferences.

**Dongsheng Yang** (M'16-SM'19) received the B.S. degree in testing technology and instrumentation, the M.S. degree in power electronics and electric drives, and the Ph.D. degree in control theory and control engineering from Northeastern University, Shenyang, China, in 1999, 2004, and 2007, respectively.

He is currently a Professor with Northeastern University. He was supported by the Program for New Century Excellent Talents in University. He has authored or coauthored around 70 papers published in academic journals and conference proceedings, 3 monographs, and co-invented 80 patents. His current research interests include distributed generation, multi energy power system, and artificial intelligence-based fault diagnosis and protection. Prof. Yang was a recipient of the Second Prize of National Science and Technology Progress.

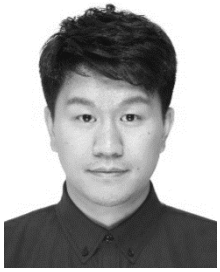

**Bowen Zhou** (S'12-M'16) received the B.Sc. and M.Sc. degrees from Wuhan University, Wuhan, China, in 2010 and 2012, respectively, and the Ph.D. degree from Queen's University Belfast, Belfast, UK, in 2016, all in electrical engineering. He joined Institute of Electric Automation, College of Information Science and Engineering, Northeastern University, Shenyang, China, in 2016, where he is currently working as an associate professor.

His research interests include power system operation, stability and control, vehicle to grid, energy storage and virtual energy storage, demand response, renewable energy, and energy internet. He is also the PI or Co-I of more than 10 government or industry sponsored projects. He has published more than 60 SCI or EI indexed papers. He is currently a member of IEEE, IET, IAENG, CSEE, CAA, and CCF. He is also a standing director or director of several IEEE PES China committees and subcommittees. He has served as session chairs and TC/PC members for more than 10 international conferences.

**Yan-Fei Liu** (F'13) received his bachelor's and master's degrees from Zhejiang University, China, in 1984 and 1987 and Ph.D. degree from Queen's University, Kingston, ON, Canada, in 1994. He was a Technical Advisor with the Advanced Power System Division, Nortel Networks, in Ottawa, Canada from 1994 to 1999. Since 1999, he has been with Queen's University, where he is currently a Professor with the Department of Electrical and Computer Engineering. His current research interests include optimal application of GaN and SiC devices to achieve small size and high efficiency power conversion, 99% efficiency power conversion with extremely high power density, digital control technologies for high efficiency, fast dynamic response dc–dc switching converter and ac–dc converter with power factor correction, resonant converters and server power supplies, and LED drivers. He has authored around 250 technical papers in the IEEE Transactions and conferences, and holds 35 U.S. patents. He has written a book on "High Frequency MOSFET Gate Drivers: Technologies and Applications," published by IET. He is also a Principal Contributor for two IEEE standards. He received "Modeling and Control Achievement Award" from IEEE Power Electronics Society in 2017. He received Premier's Research Excellence Award in 2000 in Ontario, Canada. He also received the Award of Excellence in Technology in Nortel in 1997. Dr. Liu is the Vice President of Technical Operations of IEEE Power Electronics Society (PELS, from 2017 to 2020). He is the General Chair of ECCE 2019 to be held in Baltimore, USA in 2019. His major service to IEEE is listed below: a Guest Editor-in-Chief for the special issue of Power Supply on Chip of IEEE TRANSACTIONS ON POWER ELECTRONICS from 2011 to 2013; a Guest Editor for special issues of JESTPE: Miniaturization of Power Electronics Systems in 2014 and Green Power Supplies in 2016; as Co-General Chair of ECCE 2015 held in Montreal, Canada, in September 2015; the Chair of PELS Technical Committee (TC1) on Control and Modeling Core Technologies from 2013 to 2016; Chair of PELS Technical Committee (TC2) on Power Conversion Systems and Components from 2009 to 2012.

**Huaguang Zhang** (M'03, SM'04, F'14) received the B.S. degree and the M.S. degree in control engineering from Northeast Dianli University of China, Jilin City, China, in 1982 and 1985, respectively. He received the Ph.D. degree in thermal power engineering and automation from Southeast University, Nanjing, China, in 1991.

He joined the Department of Automatic Control, Northeastern University, Shenyang, China, in 1992, as a Postdoctoral Fellow for two years. Since 1994, he has been a Professor and Head of the Institute of Electric Automation, School of Information Science and Engineering, Northeastern University, Shenyang, China. His main research interests are fuzzy control, stochastic system control, neural networks based control, nonlinear control, and their applications. He has authored and coauthored over 280 journal and conference papers, six monographs and co-invented 90 patents.

Dr. Zhang is the fellow of IEEE, the E-letter Chair of IEEE CIS Society, the former Chair of the Adaptive Dynamic Programming & Reinforcement Learning Technical Committee on IEEE Computational Intelligence Society. He was awarded the Outstanding Youth Science Foundation Award from the National Natural Science Foundation Committee of China in 2003. He was named the Cheung Kong Scholar by the Education Ministry of China in 2005. He is a recipient of the IEEE Transactions on Neural Networks 2012 Outstanding Paper Award. He is also a recipient of Andrew P. Sage Best Transactions Paper Award 2015.